focus on the spin-precession and spin-diffusion lengths. The possibility of observing and using spin precession of an ensemble of electrons in the diffusive regime is demonstrated by our numerical Monte Carlo simulations (22, 28) shown in Fig. 1C.

The numerically obtained spin-precession period is well described by an analytical formula derived from the dynamics of the spin-density matrix (28), $L_{SO} = \pi\hbar^2/m^*(|\alpha| + |\beta|)$; $m^* = 0.067$ is the electron effective mass in GaAs. There are two regimes in which spin precession can be observed in the diffusive transport regime. In one regime, the width of the channel is not relevant and a spin-diffusion length larger than the precession length occurs as a result of the single-particle transport analog of the spin helix state (9) realized at 2DEG Rashba and Dresselhaus spin-orbit fields of equal or similar strengths, $\alpha \approx -\beta$ for our bar orientation. When the two spin-orbit fields are not tuned to similar strengths, the spin-diffusion length is approximately given by $\sim L_{SO}^2/w$ and spin precession is therefore observable only when the width w of the channel is comparable to or smaller than the precession length (28–30).

The complex design of our semiconductor heterostructure provides simultaneously the means for spin injection, electrical gating, and detection, so we did not rely on further fine tuning of the internal spin-orbit fields to realize the spin helix state condition. Instead, we fabricated narrow Hall bars whose width is smaller than the precession length and used a strongly focused light spot for spin injection. As shown in Fig. 1C, several precessions are readily observable in this quasi one-dimensional geometry even in the

diffusive regime and for $\alpha \neq -\beta$, and the spin-precession and spin-diffusion lengths in this regime are independent of the mean-free-path, i.e., of the mobility of the 2DEG channel (28).

The strength of the confining electric field of the 2DEG underneath the gate changes by up to a factor of ~2 in the range of applied gate voltages in our experiments. This result implies (22) comparably large changes in the strength of the internal spin-orbit fields in the 2DEG channel. The dependence on the spin-orbit field strength shown in the above equation and confirmed by Monte Carlo simulations (28) (and the independence on the momentum of injected electrons) implies also comparably large changes in the spin-precession length. These estimates corroborate the observed spin manipulation in our spin Hall effect transistors by external electric fields applied to the gates.

References and Notes

1. I. Žutić, J. Fabian, S. Das Sarma, *Rev. Mod. Phys.* **76**, 323 (2004).
2. T. Dietl, D. D. Awschalom, M. Kaminska, H. Ohno, Eds., *Spintronics*, vol. 82 of *Semiconductors and Semimetals* (Elsevier, Amsterdam, 2008).
3. S. Datta, B. Das, *Appl. Phys. Lett.* **56**, 665 (1990).
4. J. M. Kikkawa, D. D. Awschalom, *Nature* **397**, 139 (1999).
5. H. J. Zhu et al., *Phys. Rev. Lett.* **87**, 016601 (2001).
6. P. R. Hammar, M. Johnson, *Phys. Rev. Lett.* **88**, 066806 (2002).
7. G. Schmidt, L. W. Molenkamp, *Semicond. Sci. Technol.* **17**, 310 (2002).
8. J. Schliemann, J. C. Egues, D. Loss, *Phys. Rev. Lett.* **90**, 146801 (2003).
9. B. A. Bernevig, J. Orenstein, S.-C. Zhang, *Phys. Rev. Lett.* **97**, 236601 (2006).
10. X. Jiang et al., *Phys. Rev. Lett.* **94**, 056601 (2005).
11. S. A. Crooker et al., *Science* **309**, 2191 (2005).
12. C. P. Weber et al., *Phys. Rev. Lett.* **98**, 076604 (2007).
13. X. Lou et al., *Nat. Phys.* **3**, 197 (2007).
14. B. Huang, D. J. Monsma, I. Appelbaum, *Phys. Rev. Lett.* **99**, 177209 (2007).
15. H. C. Koo et al., *Science* **325**, 1515 (2009).
16. M. I. Dyakonov, V. I. Perel, *Phys. Lett. A* **35**, 459 (1971).
17. J. E. Hirsch, *Phys. Rev. Lett.* **83**, 1834 (1999).
18. S. Murakami, N. Nagaosa, S.-C. Zhang, *Science* **301**, 1348 (2003).
19. J. Sinova et al., *Phys. Rev. Lett.* **92**, 126603 (2004).
20. Y. K. Kato, R. C. Myers, A. C. Gossard, D. D. Awschalom, *Science* **306**, 1910 (2004).
21. J. Wunderlich, B. Kaestner, J. Sinova, T. Jungwirth, *Phys. Rev. Lett.* **94**, 047204 (2005).
22. J. Wunderlich et al., *Nat. Phys.* **5**, 675 (2009).
23. Materials and methods are available on *Science* online.
24. B. Kaestner, J. Wunderlich, T. J. B. M. Janssen, *J. Mod. Opt.* **54**, 431 (2007).
25. S. O. Valenzuela, M. Tinkham, *Nature* **442**, 176 (2006).
26. C. Brüne et al., *Nat. Phys.* **6**, 448 (2010).
27. E. S. Garlid, Q. O. Hu, M. K. Chan, C. J. Palmstrøm, P. A. Crowell, *Phys. Rev. Lett.* **105**, 156602 (2010).
28. L. P. Zârbo, J. Sinova, I. Knezevic, J. Wunderlich, T. Jungwirth, *Phys. Rev. B* **82**, 205320 (2010).
29. A. A. Kiselev, K. W. Kim, *Phys. Rev. B* **61**, 13115 (2000).
30. S. Kettemann, *Phys. Rev. Lett.* **98**, 176808 (2007).
31. We acknowledge support from European Union grant FP7-215368 SemiSpinNet; Czech Republic grants AV0Z10100521, MSM0021620834, KAN400100652, LC510, and Preamium Academiae; and U.S. grants NSF-MRSEC DMR-0820414, ONR-N000140610122, DMR-0547875, and SWAN-NRI. J.S. is a Cottrell Scholar of Research Corporation. In connection with this work, we have two pending patent applications with the European Patent Office, patent numbers EP 2 224 500 A2 and EP 2 190 022 A.

Brownian Motion of Stiff Filaments in a Crowded Environment

Nikta Fakhri,[1] Frederick C. MacKintosh,[2] Brahim Lounis,[3] Laurent Cognet,[3] Matteo Pasquali[1]*

The thermal motion of stiff filaments in a crowded environment is highly constrained and anisotropic; it underlies the behavior of such disparate systems as polymer materials, nanocomposites, and the cell cytoskeleton. Despite decades of theoretical study, the fundamental dynamics of such systems remains a mystery. Using near-infrared video microscopy, we studied the thermal diffusion of individual single-walled carbon nanotubes (SWNTs) confined in porous agarose networks. We found that even a small bending flexibility of SWNTs strongly enhances their motion: The rotational diffusion constant is proportional to the filament-bending compliance and is independent of the network pore size. The interplay between crowding and thermal bending implies that the notion of a filament's stiffness depends on its confinement. Moreover, the mobility of SWNTs and other inclusions can be controlled by tailoring their stiffness.

Crowding greatly constrains the transversal mobility of a filament and causes anisotropic diffusion, which is limited to the filament axial direction. In the case of polymer solutions or melts, understanding the motion of a single polymer chain confined by the meshwork of its neighbors was key to a number of advances in polymer science. In their seminal work, de

Gennes, Doi, and Edwards (1–3) modeled the effect of crowding on polymer dynamics by introducing the concept of a confining tube, together with preferential motion along the polymer's axis, known as reptation because of its resemblance to the slithering of a snake (Fig. 1A, inset). This model captured many bulk dynamical properties of flexible polymer melts and solutions (4), al-

though direct experimental evidence validating this powerful theoretical intuition came over two decades later, when reptation of flexible and semi-flexible filaments was observed directly by imaging fluorescently labeled DNA (5) and actin (6).

In contrast, little is known about the thermal motion of stiff filaments such as carbon nanotubes, biopolymers, and stiff fibers in a network. In particular, the role of the bending stiffness of such inclusions remains controversial, with long-standing conflicting theoretical predictions (7–11). Doi predicted that rotational diffusion is independent of stiffness (7), whereas Odijk concluded that such diffusion should be enhanced by flexibility (9) and Sato concluded the opposite (11). Bulk experiments by means of birefringence and dichroism (12–14) have also given conflicting

[1]Department of Chemical and Biomolecular Engineering, Department of Chemistry, Smalley Institute for Nanoscale Science and Technology, Rice University, Houston, TX 77005, USA. [2]Department of Physics and Astronomy, Vrije Universiteit, 1081 HV Amsterdam, Netherlands. [3]Centre de Physique Moléculaire Optique et Hertzienne, Université de Bordeaux CNRS, Talence F-33405, France.

*To whom correspondence should be addressed. E-mail: mp@rice.edu

results, mainly because polydispersity, aggregation, attractive forces, and strong coupling between translational and rotational diffusivities of the filaments all complicate the interpretation of the results. We directly visualized single-walled carbon nanotubes (SWNTs) reptating in a gel and established that flexibility substantially speeds up diffusion of stiff filaments under confinement, which is in accord with Odijk's theory (9). We found that the rotational diffusion constant grows linearly with the bending flexibility and, counterintuitively, is independent of degree of crowding.

A natural measure of the stiffness of a filament is its persistence length, $L_p = \kappa/k_B T$, which measures its thermal bending by Brownian forces.

Here, κ is the bending stiffness, T is the temperature, and k_B is Boltzmann's constant. Doi (7) postulated that as long as the rods are stiff ($L < L_p$), flexibility does not affect diffusion, and that such a stiff filament of length L confined in a tube of diameter $\xi \ll L$ would explore an angle $\theta \approx \xi/L$ in the reptation time $\tau_{rep} = L^2/D_\parallel$ needed to diffuse a length L. This yields a rotational diffusivity $D_r^{Doi} = \theta^2/\tau_{rep} = k_B T \xi^2/\eta L^5$, where $D_\parallel \sim k_B T/\eta L$ is the translational diffusivity of an isolated filament in a solvent of viscosity η. In contrast, Odijk (9) argued that whenever the amplitude of the thermal undulations $u = (L^3/L_p)^{1/2}$ exceeds the pore diameter, confinement results in the independent deflection of segments of length $\lambda = (L_p \xi^2)^{1/3}$, of which there are

L/λ (15). As the filament reptates a distance λ, the ends of the filament reorient by an angle $\delta\theta \sim \xi/\lambda$. After a reptation time, this results in a mean-square angular deflection of the filament of $\theta^2 \sim \xi^2 L/\lambda^3$ and an angular diffusivity of $D_r^{Odijk} = k_B T/\eta L^2 L_p$. Doi's theory is recovered for filaments shorter than λ, a length typically much shorter than the persistence length, at which the flexibility becomes irrelevant. Otherwise, Odijk theory predicts that rotational diffusion speeds up by a factor $D_r^{Odijk}/D_r^{Doi} = (L/\lambda)^3$, for example, by three orders of magnitude for a 10-μm-long, stiff ($L_p = 100$ μm) filament moving through 100-nm pores. (9)

SWNTs are the ideal system to study confined dynamics of stiff filaments. SWNTs are slender (typical diameters of $d \approx 0.7$ to 1.2 nm), sufficiently long to be visualized through optical microscopy ($L \approx 3$ to 15 μm), and share many dynamical characteristics with polymers (17, 18). SWNTs are considered stiff because their persistence length ranges from 20 to 150 μm and scales with their diameter cubed, $L_p \sim d^3$, similar to the bending stiffness of a macroscopic hollow pipe (19). Individual semiconducting SWNTs can be visualized directly because of their bright near-infrared (NIR) luminescence, and their diameter can be determined simultaneously spectroscopically (20). We image the quasi-two-dimensional dynamics of these individual SWNTs in agarose gel (21), a permanent network with pores $\xi \approx 0.1$ to 1 μm [depending on agarose concentration (22, 23)], which mimics the reptation ansatz of a filament moving in a fixed network of frozen obstacles (1–3). The diameter (hence the persistence length) of each SWNT was determined from its emission spectrum (19, 20). By means of image analysis, we extracted frame-by-frame each SWNT's center-of-mass position $r_i = [x_i, y_i]$ in the lab coordinates and its orientation θ_i relative to the x axis (i represents the frame number spaced by 30 ms acquisition time). Figure 1A depicts the center-of-mass trajectory of a 4.5-μm-long (6,5) SWNT [deduced from its emission spectrum (Fig. 1B)], with a 0.76 nm diameter and $L_p = 26$ μm (19) in a 1.5% w/w agarose gel ($\xi \approx 0.2$ μm); this figure and the accompanying video (24) show unequivocally snake-like motion. NIR fluorescence snapshots demonstrate that flexibility substantially affects reorientation of the SWNT in a new confining tube. At first, the SWNT slides back and forth partially out of the confining tube. By bending slightly, the end of the SWNT has more freedom to explore various paths while translating along its length, even though most of the SWNT is still caged and thus restricted to a certain orientation. Eventually, the SWNT completely slides out of the original confining tube and reorients in another tube.

We quantify rotational motion by the statistics of the angle θ_i. A typical time-evolution of the mean-square angular displacement (MSAD), $\langle \Delta\theta^2 \rangle$, is shown in Fig. 1C. At short times, the SWNT's angular diffusion is subdiffusive ($\langle \Delta\theta^2 \rangle \propto \tau^n$, $n \ll 1$), reflecting the confinement in the initial tube. At longer times, the SWNT diffuses out of the initial tube, and the mean angular displacement
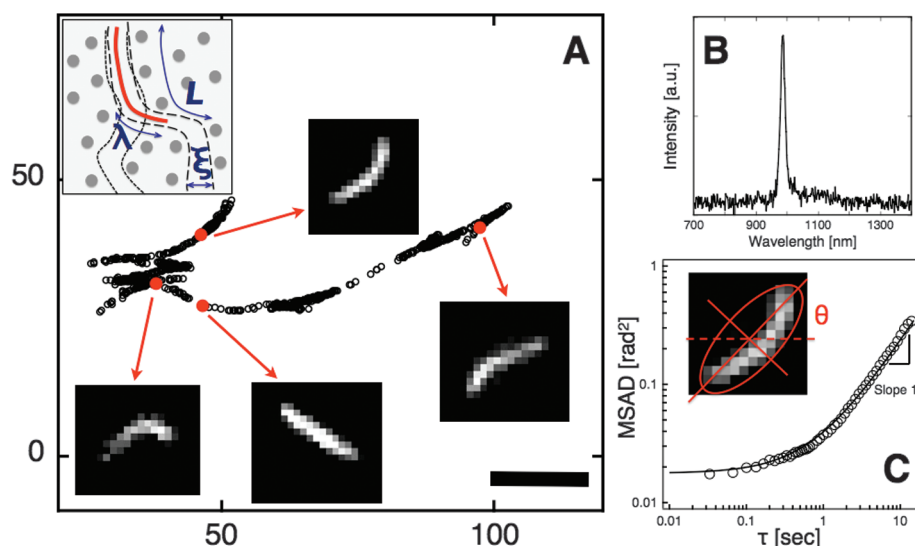

Fig. 1. (**A**) (x, y) center-of-mass trajectories of a SWNT reptating in 1.5 w/w % agarose gel and representative NIR images of the SWNT, illustrating the effect of flexibility on reorientation of SWNT in different pores (scale bar, 5 μm). (Inset) Schematic of a stiff filament in a fixed network: L is the length of the filament, λ is the deflection length, and ξ is the pore size of the network. (**B**) Individual SWNT emission spectrum with peak at 985 nm, implying a (6, 5) structure with a diameter of 0.76 nm and persistence length of 26 μm. (**C**) Angular MSD showing the subdiffusive-to-diffusive behavior which occurs at disengagement time τ_d. The line is the best fit to the data. D_r is calculated from the long time (diffusive behavior). (Inset) Representative image of a SWNT in x-y lab frame; the orientation angle θ is the angle between the x axis and the major axis of the best-fitted ellipse to the shape of the SWNT.

Fig. 2. Normalized rotational diffusivity of 35 SWNTs with different length and persistence length [denoted by different symbols (table S1)], reptating in different concentrations of agarose gel versus normalized length by deflection length. Doi's theory is shown by a dashed line and predicts a power law with scaling exponent −3 across the whole range of normalized length. Odijk's theory is denoted by a solid line and predicts a plateau at ~1 for $L > \lambda$.
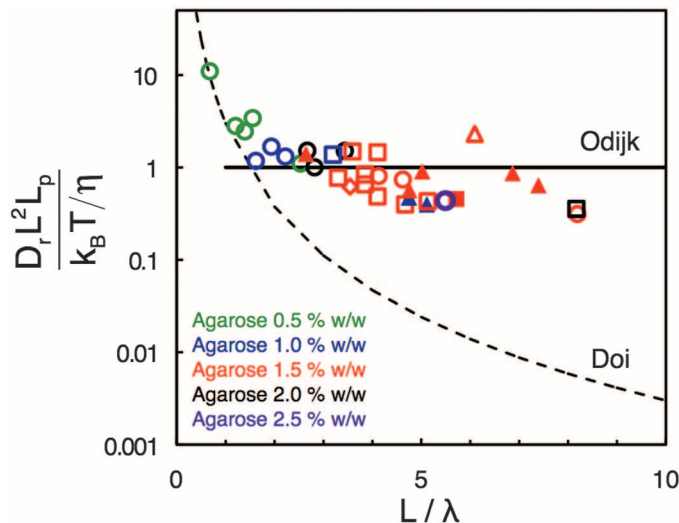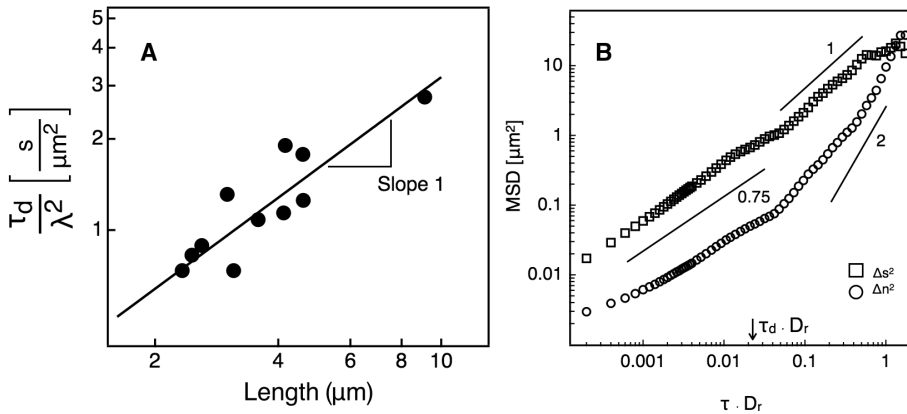
Fig. 3. (A) The disengagement time normalized by deflection length λ^2 scales linearly with length L. **(B)** Time domains in translational MSDs parallel (Δs^2) and perpendicular (Δn^2) to the time-averaged reptation path (corresponding to the SWNT in Fig. 1A). $\tau < \tau_d$ is the dynamics inside the tube. $\tau_d < \tau < \tau_r$ is the crossover region between anisotropic and isotropic diffusion. $\tau > \tau_r$ is the isotropic diffusive long-time dynamics.

behaves diffusively $\langle \Delta\theta^2 \rangle = 2D_r\tau$ (25), yielding the value of the rotational diffusivity D_r.

We measured the rotational diffusivity of 35 SWNTs with different lengths (2 to 10 μm) and persistence lengths (26 to 60 μm), reptating in agarose gels of several concentrations (hence pore sizes). We collapsed the rotational diffusivity on a master curve (Fig. 2) by plotting the normalized rotational diffusivities $D_r / D_r^{\text{Odijk}} = D_r\eta L^2 L_p/k_B T$ versus normalized length L/λ. In such a plot, Doi's theory predicts a power law with scaling exponent -3 $[(L/\lambda)^{-3}]$ across the whole range of normalized length (Fig. 2, dashed line), whereas Odijk's theory predicts a plateau at ~1 for $L > \lambda$ (Fig. 2, solid line). The data show that when $L \geq \lambda$, flexibility does not affect mobility (which is in agreement with both Doi and Odijk), whereas for $L > \lambda$ flexibility clearly speeds up long-time diffusion, which follows Odijk's scaling. Therefore, the effective rigidity of a filament depends on its degree of confinement. Whereas in the absence of confinement Brownian filaments can be considered essentially as rigid when $L < L_p$, confined filaments ($\xi < L$) behave as rigid when $L > \lambda$.

We next turned to the short-time subdiffusive dynamics of the MSAD (Fig. 1C). To cross over from short time subdiffusive behavior to long-time diffusive motion, a filament must diffuse by a length λ out of its initial confining tube. This occurs on a time scale known as the disengagement time τ_d, which is the time scale a SWNT needs to reptate by a deflection length and is determined from the free parallel diffusion constant of the center of the mass, $\tau_d = \lambda^2/D_{\parallel} \sim \eta\lambda^2 L/k_B T$ (9). At times shorter than τ_d, the SWNT wiggles "freely" inside its initial confining tube, with minimal angular reorientation ($\theta < \xi/L$, hence the subdiffusive behavior of MSAD in Fig. 1C). At times longer than τ_d, the SWNT slides out of the initial confining tube and starts exploring the other accessible tubes. Show in Fig. 3 are the disengagement times normalized to λ^2 obtained for 11 (6,5) SWNTs by fitting the MSAD with $\langle\Delta\theta^2\rangle = \theta_0^2 + 2D_r\tau$ and setting $\tau_d = \theta_0^2/2D_r$. We

found that the measured τ_d normalized by deflection length λ^2 scales linearly with length L, confirming Odijk's prediction (9) for short-time translational diffusion (26) and showing that flexibility speeds up disengagement.

Because SWNTs explore orientation space by reptating in and out of pores, rotational and translational diffusion should be strongly coupled at time scales below the rotational diffusion time $\tau_r = 1/2D_r$. Such coupling occurs even in the much simpler case of two-dimensional Brownian motion of an unconstrained ellipsoid and is well described in terms of Perrin-Smoluchowski theory (27). Theoretical calculations and simulations have recently shown that this same theory can capture such coupling in the motion of confined rigid rods (infinite L_p) (28). To investigate this coupling experimentally, we measured the time evolution of the center-of-mass mean square displacements (MSDs) parallel (Δs^2) and perpendicular (Δn^2) to the orientation of the reptation tube, averaged over the same time window (23). The parallel and perpendicular MSDs versus time (normalized by the rotational diffusion time) are shown in Fig. 3B.

At short times ($\tau < \tau_d$), SWNT diffusion is anisotropic—$\Delta s^2 \gg \Delta n^2$; SWNTs diffuse much faster parallel than perpendicular to the tube axis. In this time regime, the dynamics of center of mass is dominated by the relaxation of thermally excited elastic bending modes of the SWNT, with relaxation times $\tau_r^n \sim \eta l_n^4/\kappa$, where l_n is the mode wavelength (29). For a given time τ, long-wave modes ($\tau_r^n > \tau$) are effectively "frozen," whereas short-wave modes ($\tau_r^n < \tau$) evolve and contribute to the amplitude of thermal undulations. At time τ, the longest (dominant) bending mode has a wavelength of $l(\tau) \sim (\kappa\tau/\eta)^{1/4}$. The mean square amplitude of the transverse fluctuations (Δu^2) of this mode dominate the transverse diffusion of the center of mass and evolves with time (29–31) as $\Delta u^2 \approx \Delta n^2 \sim l(\tau)^3/L_p \sim \tau^{3/4}$, which is indeed the subdiffusive power law $\tau^{3/4}$ we measured (Fig. 3B). The same time dependence, $\tau^{3/4}$, is also expected for the mean square amplitude of the

longitudinal fluctuations of the SWNT (29, 31); these dominate the mean square longitudinal displacement of the center of mass Δs^2, as shown in Fig. 3B. At longer times, Δs^2 crosses over to a linear diffusion regime, indicating that the SWNT has fully reptated along its length ($\Delta s^2 \sim \tau$). In this crossover regime, the transverse MSD Δn^2 grows super-linearly with time because reptation occurs along a curved path—a motion that couples rotation and translation ($\Delta n^2 \sim D_{\parallel}\tau\Delta\theta^2 \sim D_{\parallel}D_r\tau^2$) (10, 28). Thus on intermediate time scales between disengagement and rotational diffusion times (τ_d and τ_r), translational diffusion perpendicular to the filament is also enhanced by flexibility. At times longer than rotational diffusion time τ_r, the SWNT loses memory of its initial orientation, and its diffusion becomes isotropic. On these time scales, translational diffusion is weakly reduced by flexibility (32).

By varying SWNT surface modifications (33), we can selectively tune the sensitivity of the carbon nanotubes to the different physical properties of the porous media for transport and sensing applications (such as a cellular crowded environment). The orientation dynamic behavior of SWNTs in a fixed network is a starting point to study the dynamics of concentrated solutions of SWNTs as well as SWNT composite materials. Our results indicate that the SWNT shapes are altered by the presence of the pores and that bent shapes can be very long lived. Rotational diffusion and coupling between translational and rotational motion of SWNTs can provide a useful counterpart to translational diffusion approaches in microrheology techniques and render the ability to probe different viscoelastic modes or local heterogeneity in complex fluids and biological media.

References and Notes
1. P. G. de Gennes, *J. Chem. Phys.* **55**, 572 (1971).
2. M. Doi, S. F. Edwards, *J. Chem. Soc., Faraday Trans. II* **74**, 1789 (1978).
3. S. F. Edwards, *Proc. Phys. Soc. Lond.* **92**, 9 (1967).
4. M. Doi, S. F. Edwards, *The Theory of Polymer Dynamics* (Oxford Univ. Press, Oxford, 1986).
5. T. T. Perkins, D. E. Smith, S. Chu, *Science* **264**, 819 (1994).
6. J. Käs, H. Strey, E. Sackmann, *Nature* **368**, 226 (1994).
7. M. Doi, *J. Phys.* **36**, 607 (1975).
8. F. Höfling, T. Munk, E. Frey, T. Franosch, *Phys. Rev. E Stat. Nonlin. Soft Matter Phys.* **77**, 060904R (2008).
9. T. Odijk, *Macromolecules* **16**, 1340 (1983).
10. S. Ramanathan, D. C. Morse, *Phys. Rev. E Stat. Nonlin. Soft Matter Phys.* **76**, 010501 (2007).
11. M. Sato, Y. Takada, A. Teramoto, *Macromolecules* **24**, 6220 (1991).
12. M. Tracy, R. Pecora, *Annu. Rev. Phys. Chem.* **43**, 525 (1992).
13. S. S. Wijmenga, A. Maxwell, *Biopolymers* **25**, 2173 (1986).
14. K. M. Zero, R. Pecora, *Macromolecules* **15**, 87 (1982).
15. This characteristic length scale has been estimated from thermal fluctuations of flexible filaments in an ordered polymer background (16).
16. Z. Dogic et al., *Phys. Rev. Lett.* **92**, 125503 (2004).
17. M. J. Green, N. Behabtu, M. Pasquali, W. W. Adams, *Polymer (Guildf.)* **50**, 4979 (2009).
18. R. Duggal, M. Pasquali, *Phys. Rev. Lett.* **96**, 246104 (2006).
19. N. Fakhri, D. A. Tsyboulski, L. Cognet, R. B. Weisman, M. Pasquali, *Proc. Natl. Acad. Sci. U.S.A.* **106**, 14219 (2009).
20. D. A. Tsyboulski, S. M. Bachilo, R. B. Weisman, *Nano Lett.* **5**, 975 (2005).
21. L. Cognet et al., *Science* **316**, 1465 (2007).

22. T. K. Attwood, B. J. Nelmes, D. B. Sellen, *Biopolymers* **27**, 201 (1988).
23. N. Pernodet, M. Maaloum, B. Tinland, *Electrophoresis* **18**, 55 (1997).
24. Materials and methods are available as supporting material on *Science* Online.
25. Rotational diffusion is characterized in two dimensions by a single diffusion coefficient, D_r, and associated diffusion time, $\tau_r = 1/2D_r$.
26. The errors introduced by the limited angular resolution in our measurements can affect the interpretation of the short time dynamics. The microscope angular resolution is $\approx a/L$, where a is the pixel size. Therefore, resolution limits our experiments below a resolution time of $\tau_{resolution} \cong a^2 L_p \pi \eta/2k_B T$. In the experimental conditions of Fig. 3A, $\tau_{resolution}/\tau_d = [(\lambda/L)(a/\xi)^2]/4$ ranges from 0.01 to 0.26; therefore, $\tau_{resolution} << \tau_d$ and resolution does not substantially affect the measurement of the subdiffusive regime due to the short-time dynamics in the system.
27. Y. Han *et al.*, *Science* **314**, 626 (2006).
28. T. Munk, F. Hofling, E. Frey, T. Franosch, *Europhys. Lett.* **85**, 30003 (2009).
29. F. Gittes, F. C. MacKintosh, *Phys. Rev. E Stat. Phys. Plasmas Fluids Relat. Interdiscip. Topics* **58**, R1241 (1998).
30. E. Farge, A. C. Maggs, *Macromolecules* **26**, 5041 (1993).
31. R. Granek, *J. Phys. II* **7**, 1761 (1997).
32. M. Doi, *J. Polymer Sci. Polymer Symp.* **73**, 93 (1985).
33. J. G. Duque *et al.*, *J. Am. Chem. Soc.* **130**, 2626 (2008).
34. This work was supported by the NSF Center for Biological and Environmental Nanotechnology (EEC-0118007 and EEC-0647452), the Welch Foundation (grant C-1668), the Advanced Energy Consortium (www.beg.utexas.edu/aec), the Région Aquitaine, the Agence Nationale pour la Recherche (ANR PNANO), the European Research Council (grant n 232942), and the Foundation for Fundamental Research on Matter (FOM), which is part of the Netherlands Organisation for Scientific Research (NWO).

Tunable Field Control Over the Binding Energy of Single Dopants by a Charged Vacancy in GaAs
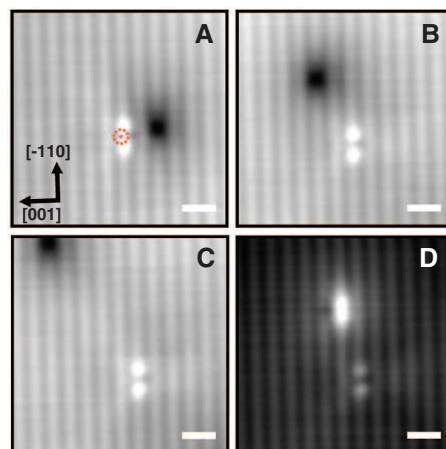
D. H. Lee and J. A. Gupta*

Local manipulation of electric fields at the atomic scale may enable new methods for quantum transport and creates new opportunities for field control of ferromagnetism and spin-based quantum information processing in semiconductors. We used a scanning tunneling microscope to position charged arsenic (As) vacancies in the gallium arsenide 110 [GaAs(110)] surface with atomic precision, thereby tuning the local electrostatic field experienced by single manganese (Mn) acceptors. The effects of this field are quantified by measuring the shift of an acceptor state within the band gap of GaAs. Experiments with varying tip-induced band-bending conditions suggest a large binding energy for surface-layer Mn, which is reduced by direct Coulomb repulsion when the As vacancy is moved nearby.

The scaling of electronic devices such as field-effect transistors to nanometer dimensions requires more precise control of individual dopants in semiconductor nanostructures, because statistical fluctuations in dopant distributions are beginning to affect the performance and functionality of current devices (1–4). Proposals for next-generation quantum- and spin-based electronics also rely on the tuning of the charge, spin, and interactions of dopant atoms with local electric fields [e.g., P in Si (5) or Mn in GaAs (6)]. On Si surfaces, the scanning tunneling microscope (STM) has been used to probe the influence of charged dangling bonds on molecular conductance (7). In III-V semiconductors, recent STM studies of single Si, Zn, and Mn dopants have shown that the electronic and magnetic properties of such impurities depend on proximity to the surface (8–14), other impurities (15), interactions with the STM tip (9, 14, 16, 17), and local strain fields (18).

Here, we demonstrate control of single-dopant properties by using the local electrostatic field emanating from a charged vacancy. Using an STM, we can position this vacancy with atomic precision or reversibly switch it to a neutral state to tune the binding energy of holes to individual Mn acceptors in GaAs. Experiments were performed with a custom-built ultra-high vacuum (UHV) STM operated at 7.3 K (19). The semiconductor sample is a commercial p-GaAs wafer doped with 2×10^{18} cm^{-3} Zn atoms for nonzero conductivity at low temperature.

Arsenic vacancies, V_{As}, in the GaAs(110) surface formed during cleavage appeared as dark depressions at negative sample voltage (e.g., Fig. 1A) and could be positioned on the surface by applying a positive voltage pulse (~+1.7 V) (fig. S1). Fig. 1, A to C, shows STM images with V_{As} at three different positions. The average distance (~8 Å) and direction of the motion could not always be controlled and changed with different atomic-scale terminations of the STM tip. Thermal- and electro-migration of V_{As} have been studied previously by STM (20, 21).

The nanometer-scale depression around V_{As} reflects downward band bending associated with its +1e charge in p-GaAs (20). However, we could reversibly switch V_{As} to a neutral state by applying a smaller voltage pulse (~+1.3 V). The neutral state of V_{As} in Fig. 1D appears as a protrusion, in contrast to the apparent depression in Fig. 1, A to C. We suggest that this state results from the capture of a tunneling electron by V_{As}^+. The neutral state is stable indefinitely at 7 K but is readily switched back to V_{As}^+ by the STM tip under typical imaging conditions.

We studied the influence of the electrostatic field provided by V_{As} on single Mn acceptors, which were formed using an STM-based substitution technique (15). Mn adatoms adsorbed onto the surface at 7 K were exchanged with Ga atoms
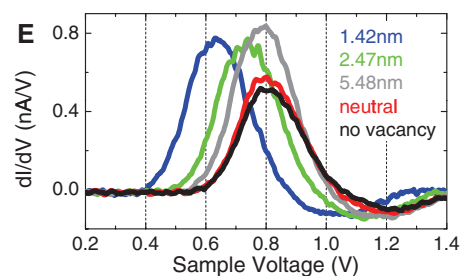

Fig. 1. Shift of Mn acceptor resonance due to V_{As}. (**A** to **D**) STM topographic images of a Mn acceptor and As vacancy in the (110) surface layer of p-GaAs ($V = -1.3$ V, $I = 0.5$ nA). Scale bar, 1 nm. Under these imaging conditions, the bright dumbbell-like shape of the Mn acceptor reflects the influence on neighboring As atoms (15). The Mn atomic position is indicated with a circle in (A). Positively charged V_{As} appears as a dark depression. (A to C) Manipulation of V_{As}^+ to three positions (1.42 nm, 2.47 nm, and 5.48 nm from Mn). (D) A voltage pulse switches the vacancy to a neutral state, which is imaged as a protrusion. (**E**) Corresponding differential conductance (dI/dV) spectra taken on the Mn acceptor. The in-gap resonance associated with the Mn acceptor shifts toward lower voltage as V_{As}^+ is moved closer. The peak shifts back to its unperturbed position when V_{As} is switched to the neutral state.

Department of Physics, Ohio State University, Columbus, OH 43210, USA.

*To whom correspondence should be addressed. E-mail: gupta.208@osu.edu